Ninth Quarterly Progress Report
N01-DC-6-2111

The Neurophysiological Effects of Simulated Auditory Prosthesis Stimulation

C.A. Miller, P.J. Abbas, J.T. Rubinstein,
B.K. Robinson and A.J. Matsuoka

Departments of Otolaryngology - Head & Neck Surgery,
Speech Pathology & Audiology, Physiology & Biophysics
The University of Iowa
Iowa City, IA 52242

January 26, 1999

Contents

List of Figures

1 Introduction

The purpose of this contract is to explore issues involving the transfer of information from implantable auditory prostheses to the central nervous system. Our investigation is being pursued along multiple parallel tracks and include the use of animal experiments and computer model simulations to:

1. Characterize fundamental spatial and temporal properties of intracochlear stimulation of the mammalian auditory nerve.
2. Evaluate the use of novel stimuli and electrode arrays.
3. Evaluate proposed enhancements in animals with a partially degenerated auditory nerve.

In this ninth quarterly progress report, we focus on new results obtained through analyses of single-fiber data obtained from a pool of cat preparations. This QPR covers two major areas:

1. a description of how single-fiber measures covary.
2. the development of a new, phenomenological, computational model that describes the whole-nerve response based upon underlying single-fiber response patterns.

In an earlier report (QPR 6), we presented single-fiber data from several cat preparations. In this ninth QPR, we extend and complete those results by presenting more thorough analyses over a larger number of fibers. This larger pool of data has also enabled us to develop the phemenological model that is presented here.

2 Summary of activities in the ninth quarter

In our ninth quarter (October through December, 1998), the following activities related to this contract were completed:

- We attended and presented at the 29th Neural Prosthesis Workshop in Bethesda, Maryland.
- Continued noise-deafening of guinea pigs to be used in studies of chronically deafened and neurally degenerated animals.

- Acquired single-fiber and EAP data from a chronically deafened cat to obtain electrophysiological data from a degenerated nerve of that species (data will be presented in a subsequent report)
- Completed extensive computational modeling of neural responses to SAM pulse trains with and without the presence of conditioning stimuli
- Submitted a manuscript for publication exploring relationships between electrically evoked single- fiber responses and the gross, whole-nerve response.
- Based in part on results obtained under this contract, we received a $150K grant from Braintronics, Inc. to study the effects of high rate pulsatile round window stimulation on human subjects with tinnitus and high frequency sensorineural hearing loss. If tinnitus in such subjects is due to loss or alteration of spontaneous activity in the basal cochlea (as suggested by others: Kiang et al., 1970) then production of pseudospontaneous activity with high rate pulse trains (Rubinstein et al., 1999) may ameliorate the tinnitus. A feasability IDE is currently being prepared.

3 Analysis of single-fiber data

In this section, we present data showing how basic single-fiber measures relate to each other across a large ensemble of fibers. We provide an interpretation of these data that suggests likely modes of membrane depolarization across the fiber ensemble. Such data provides insight on issues involving sites of action potential initiation that have interested researchers for some time.

3.1 Modes of single-fiber excitation

An assessment of information transfer from a prosthetic device to nerve fibers requires understanding how the fibers are depolarized by the electrical stimulus. One approach to this problem is to examine the pattern of responses obtained from a population of fibers. We have obtained and analyzed data from 257 fibers of 14 cats. Methodology has been previously described (see QPR #1 and #3). In most cases, single-fiber data were obtained using 39 μs monophasic pulses delivered by a monopolar electrode positioned in the basal turn of the cochlea. Response properties included

threshold, latency, jitter, and relative spread (see Verveen (1961) or QPR #3 for more on the relative spread measure). In QPR #6, we presented several interesting single-fiber phenomena. In this report, we concentrate on the group trends observed by analyses across fibers from all cats. Significant trends that were previously reported in QPR #6 (such as stimulus polarity effects) still hold and will not be presented again here.

One of our working hypotheses has been that single fibers of the mammalian auditory nerve are excitable at different longitudinal sites, perhaps at their peripheral ("dendritic") and central ("modiolar") axonal processes. We analyzed the fiber responses in light of this hypothesis to try to discern how fibers are stimulated by an intracochlear, monopolar electrode. Such data would help confirm model predictions as well as advance our general understanding of modes of excitation. We suspected that four single fiber properties threshold, mean latency, jitter, and relative spread would covary in manners consistent with different membrane properties and stimulus-dependent activating functions. To varying degrees, the four measures reflect properties of the nerve fiber membrane. For example, membrane capacitance and leakage resistance, elements affecting the membrane time constant, may influence each measure. Both of these properties vary with the degree of myelination, which is known to vary along the peripheral- to-central dimension of mammalian auditory nerve fibers (Liberman and Oliver, 1984; Spoendlin and Schrott, 1989). Similarly, axonal resistance, which is inversely proportional to fiber diameter, may also influence each measure. This property also varies with longitudinal position. Thus, these four measures may undergo systematic changes as the site of excitation varies. We might expect that excitation of membrane with relatively large membrane capacitance will produce longer spike latencies and greater relative spread. Jitter may also be expected to be greater for relatively noisy excitation sites. However, some of these measures - particularly threshold - likely depend highly upon the relative position of the electrode and the target neuron.

A test of this hypothesis requires investigation of the relationships among the four measures. In this analysis, threshold, jitter, and mean latency are reported for the 50% FE condition. We restricted the analysis to the more plentiful set of fibers stimulated with 39 μs cathodic pulses (fewer fibers responded to anodic stimuli). Since absolute sensitivity to stimuli varied somewhat across cats, single-fiber thresholds were computed relative to the stimulus level eliciting an EAP amplitude one-half that of the maximum (saturation) amplitude. Measures of mean latency, jitter, RS, and threshold are plotted versus each other in Fig. 1 for all such fibers. A linear regression

fit is included in each plot of the figure. Although the plots exhibit considerable scatter, the regressions over each set indicate statistically significant ($p < 0.05$ in all cases) correlations between each of the four measures.

The three dimensional graph of Fig. 2 presents an alternate view of the data presented in the six graphs of Fig.1. It serves to summarize the interrelationships among the four single-fiber measures. Individual fiber data are not shown; rather, single-fiber RS values are averaged into small, uniform, regions of jitter and latency. The resolution of threshold data is also reduced to three categories for this presentation, with threshold denoted by the shading of each bar. Over most of the area defined by the jitter-latency (i.e., horizontal) plane, fibers have relatively low RS values and moderate-to-high thresholds. However, fibers with the longest latencies are characterized by high jitter and RS and low-to-moderate thresholds.

Site of excitation issues may also be examined through *within-fiber* comparisons of response measures across the two stimulus polarities. It is plausible that fibers exhibiting the greatest across-polarity differences in latency may also display relatively large across-polarity differences in the other response characteristics. Our reasoning here is that the large latency differences correspond to relatively large distances between the two excitation sites. Owing to the longitudinal changes in fiber anatomy, this increases the likelihood that the two sites have differing properties. In Fig. 3, across-polarity differences in threshold, jitter, and RS are plotted as functions of the difference in latency between the two polarities. Again, the stimulus was a 39 μs pulse. Threshold, jitter, and RS measures are plotted on the ordinate as differences obtained between cathodic and anodic stimulus conditions. In each of these plots, there is a statistically significant ($p<0.001$) linear relationship between each differential measure and across-polarity latency difference. Inclusion or exclusion of the outlying datum at the far left in each graph does not affect the significance of these correlations.

The above data suggests that the cathodic excitation sites are more peripheral and noisier than the anodic sites. An important question is where the anodic and cathodic sites reside relative to the fiber's cell body. There are three possibilities: 1) both the cathodic and anodic sites are peripheral to the cell body, 2) both sites are central to the cell body, or 3) the cathodic site is peripheral to the cell body while the anodic site is central to the soma. A clue to resolving this is provided by the bimodal post-stimulus-time (PST) histograms that we reported in QPR #3. We have recorded bimodal histograms from a total of six fibers (which amounts to only about 2% of our sampled population). Examples of such histograms from two such

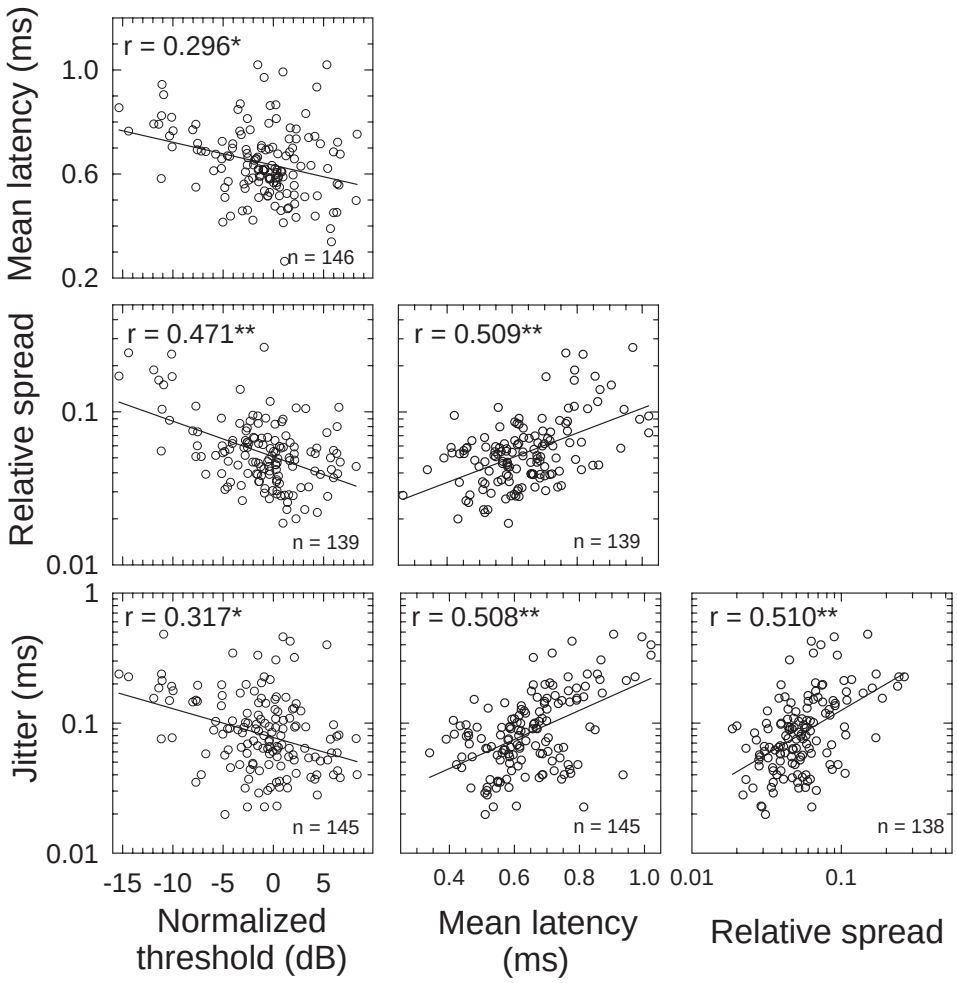

Figure 1: Regression analyses of single- fiber data obtained using 39 μs monophasic pulses delivered by a monopolar electrode positioned in the basal turn of the cochlea. Shown are scatter plots and linear regression lines for each of four response properties obtained for each fiber. Correlation coefficient and number of data are shown in each graph.

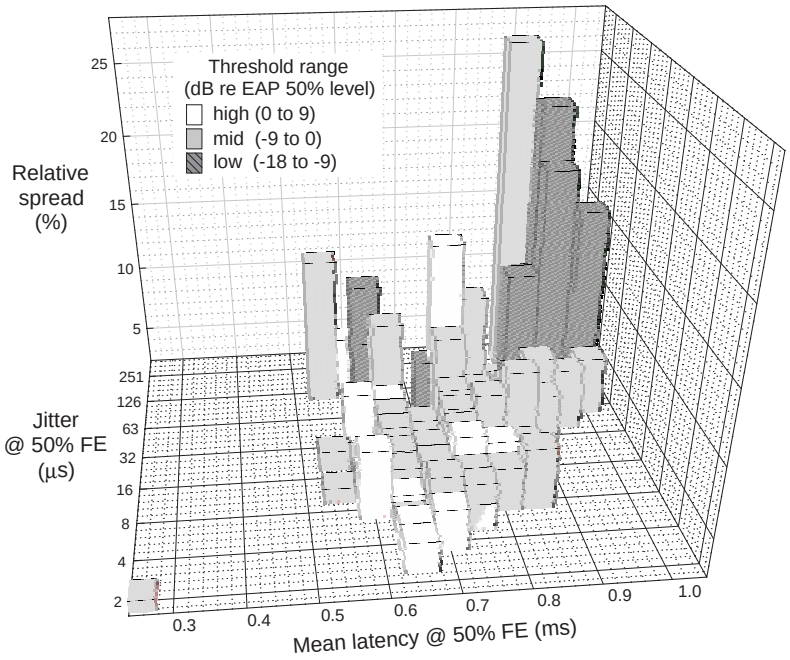

Figure 2: An alternative depiction of the data shown in Figure 1. Each bar represents the mean RS value computed over uniform areas defined by the jitter-latency plane. Mean threshold level is indicated by the shading of the bars.

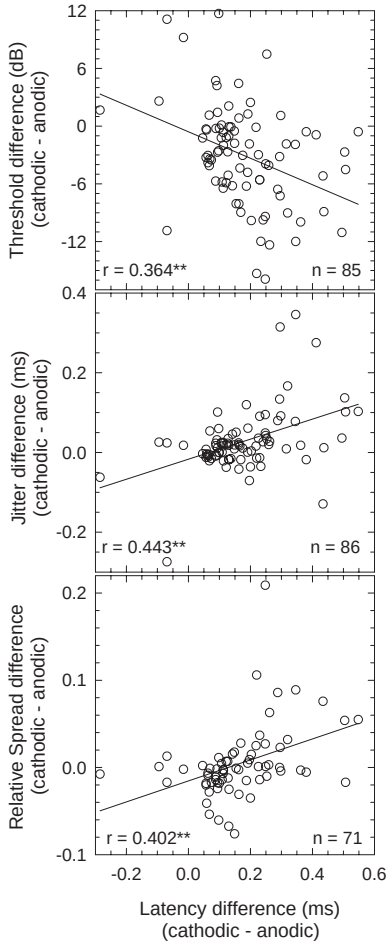

Figure 3: Plots demonstrating how within-fiber threshold, jitter, and RS vary across stimulus polarity. Threshold (top), jitter (middle), and RS (bottom) are expressed as the difference in the measures obtained with cathodic and anodic stimuli. These difference measures are plotted as a function of the difference in mean latency (at 50% FE) obtained with cathodic and anodic stimulation. Shown in each graph are linear regression fits, correlation coefficients, and the number of data. The asterisks (**) indicate that, in each case, the two plotted variables are correlated with an error probability of 0.001. Inclusion or exclusion of the leftmost datum in the plots does not change the significance of the regressions.

fibers is shown in Fig. 4. As discussed in QPR #3, our interpretation of these histograms is that they arise from spike excitation sites that bridge the cell body of the stimulated auditory nerve fiber. If that is the case, the time difference between the two peaks (labeled in the figure as "IML", for "intermodal latency") represents the conduction time across the cell body.

We suggest that, in order for peripheral cathodic excitation and central anodic excitation to occur, the mean latencies for the two stimulus polarities must be equal to or greater than the intermodal latencies observed in the bimodal- histogram fibers. This comparison is afforded by Fig. 5. The main graph of this figure depicts, for 62 fibers, the latency difference for cathodic and anodic stimuli as a function of firing efficiency. Along with those latency difference functions are plotted the mean and median values across all fibers. In addition, the intermodal latencies obtained from the six bimodal-histogram fibers are shown along the right-hand margin of the graph. If the latency difference between the two modes of the bimodal fibers were significantly greater than those observed across stimulus polarities, we could confidently state that the anodic and cathodic excitation sites do not typically reside on opposite sides of the cell body. For the six bimodal fibers encountered, the differences between the early and late modes ranged between 0.125 and 0.245 ms. As seen in Fig. 5, this range fell within the latency differences observed across the two stimulus polarities. Of the 62 fibers plotted in Fig. 5, about 35% have across-polarity latency differences (at 50% FE) less than the minimum inter-modal latency difference (0.125 ms), suggesting that it is unlikely, at least in those fibers, that opposite sides of the cell body are excited with our cathodic and anodic stimuli. We therefore conclude that, for a considerable number of fibers, the anodic and cathodic excitation sites are on the same side of the cell body. Given the location of the stimulating electrode relative to the array of cochlear fibers, we believe it likely that most fibers are excited along their central processes for both stimulus polarities, while a minority may respond with both peripheral and central excitation sites.

We hypothesized that the four single-fiber measures may show systematic changes through experimental manipulation of stimulus level and polarity. The correlations demonstrated for the scatter plots of latency, jitter, RS, and threshold (Fig. 1) support this notion for cathodic stimulation. Taken together, these plots suggest a distribution of fibers with, on one extreme, low thresholds and large values of latency, jitter, and RS. On the other extreme are fibers with high thresholds and small values of latency, jitter, and RS. Furthermore, the data are consistent with the hypothesis that the

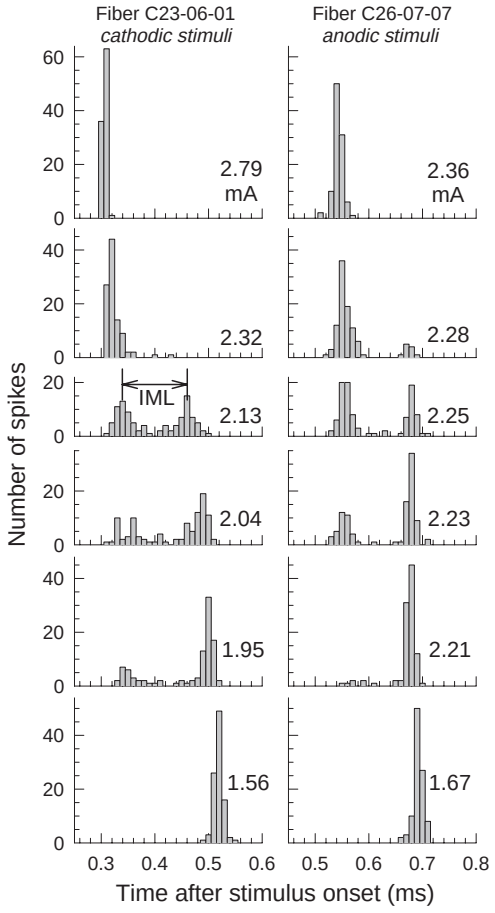

Figure 4: Post-stimulus time histograms of two fibers with level-dependent, bimodal distributions. In all cases, 39 μs monophasic stimuli were presented a total of 100 times and the fibers responded at FE = 100%. Bimodal histograms were generated with only one stimulus polarity in each case. Data in the left column were obtained using cathodic pulses while those in the right column were evoked with anodic stimulation. Stimulus level is indicated by the parameter. In each bimodal fiber that produced a histogram with both distributions, we computed an "inter-modal latency", as indicated by the double arrow labeled "IML".

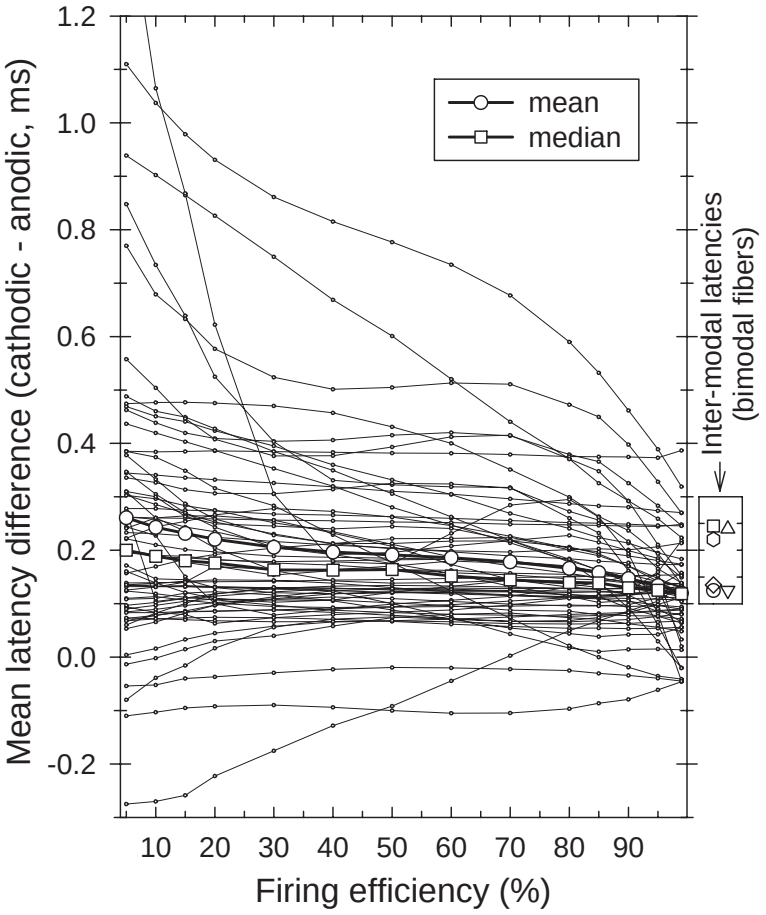

Figure 5: Comparison of the difference in mean latencies obtained with anodic and cathodic pulses and the intermodal latency differences obtained from fibers with bimodal PST histograms. Plots of the main graph were derived from the data of 62 fibers stimulated with 39 μs pulses; here, the differences between cathodic and anodic mean latencies are plotted vs. FE. In our studies, only six fibers (about 2% of all) produced bimodal PST histograms. The latency between the two modes apparent in each fiber's histogram ("Inter-modal latency") is plotted along the right margin of the graph for comparison.

fibers sampled are not uniformly distributed along the various dimensions of single-fiber response properties. When these measures are plotted versus threshold or latency, there appears to be a small number of fibers segregated into a region with long latencies, low thresholds, high jitter, and high RS. In the case of fiber responses to anodic stimulation, the interrelationships among the various measures are somewhat weaker, although in the same direction as those evident with cathodic stimulation.

Given the scatter inherent in the plots of Fig. 1, we somewhat cautiously offer the following conjectures. The distribution of fibers in these plots is consistent with the notion that, with cathodic stimulation, a small subpopulation of fibers is excited at the peripheral neuronal processes, while most are stimulated more centrally. The fact that the fibers with the longest latencies generally also have large jitter and RS values is consistent with the anatomical position and properties of the more peripheral axonal segments. Furthermore, we assume that this group of fibers has generally the lowest thresholds because of the relative proximity of their processes to the stimulating electrode. The fact that we failed to observe similar two-part distributions with anodic stimulation is consistent with the hypothesis that anodic excitation occurs at sites central to the cathodic sites. However, the lack of a two-part distribution in the anodic scatter plots may simply be an artifact of the smaller sample size of fibers stimulated with this polarity.

The plots of Fig. 3 illustrate how differences in measures of latency, jitter, and RS obtained with the two stimulus polarities vary with the difference between cathodic and anodic latency. We presume that fibers with the greatest across-polarity latency difference would demonstrate the greatest differences in the other measures because the anodic and cathodic excitation sites are presumably relatively distant from each other. In each of the three scatter plots, linear regression over the data is consistent with this notion. If we assume that the anodic excitation site is relatively constant over the range of tested stimulus levels, the range of latency differences present in plots of Fig. 2 are primarily due to shifts in the cathodic excitation site. In that case, fibers with the greatest across-polarity latency differences are those with the most peripheral cathodic excitation sites. Based on our assumptions, those fibers would also be expected to have relatively low thresholds, high jitter, and high RS, as indeed indicated by the trends of Fig. 2. We note that many fibers of Fig. 2 have similar jitter for both stimulus polarities, with a small population having greater cathodic jitter. This is again consistent with our notion that most fibers are excited by cathodic and anodic stimuli at neural sites having similar membrane properties. Finally, a

few (5 of 86) of the fibers of Fig. 2 had mean anodic latencies that were greater than their mean cathodic latencies. This, together with the example of a bimodal post-stimulus-time histogram with anodic stimulation (see QPR #3, Fig. 7), suggests that, in some cases, anodic stimulation can excite the peripheral neuronal process. Given the spiral anatomy of the cochlea, a wide range of fiber-to-electrode orientations may exist. Also, electrical inhomogeneities within the cochlea may also produce activating functions that differ markedly from that suggested by Rattay (1986). These two factors may make possible the excitation of peripheral processes with anodic stimuli.

4 A phenomenological model of the EAP

4.1 General approach

We have recently developed a phenomenological model of the EAP based upon the single-fiber response properties outlined in the previous section. In this approach, estimates of a single-fiber threshold distribution, temporal properties (i.e., latency and jitter), and firing probability are modeled to allow us to estimate a compound poststimulus time histogram ("compound PST histogram") that describes the temporal pattern of action potentials generated by the ensemble of modeled fibers at any stimulus level. The distribution and temporal properties of the modeled compound PST histogram are therefore based directly upon data gleaned from our cat preparations. The compound PST histogram, in turn, is convolved with an estimate of the "unit potential," that is, the potential generated by a single fiber that is recorded by a gross electrode (Kiang et al. , 1976) to derive the compound action potential seen by that same electrode (Goldstein and Kiang, 1958; Wang and Kiang, 1978; Wang, 1979). From the compound PST histogram we can compute the total spike count (i.e., number of spikes produced by all fibers) at any stimulus level. Thus, we are able to estimate and compare total neural activity with the summated electrical response, as described by the derived electrically evoked compound action potential ("derived EAP"). We hypothesize that level-dependent jitter and latency effects (described in Section III above) will result in a derived EAP that underestimates total spike activity. Thus, among other things, this model enables us to parse out the single-fiber properties that most influence how the EAP grows with increasing stimulus level.

4.2 Model methodology

4.2.1 General description

The main components of the computational model are described in this section. Briefly, in an iterative loop, the model computed post-stimulus-time histograms for each fiber within an empirically derived threshold distribution function. These PST histograms were defined for each fiber at each modeled stimulus level. For each fiber, histograms were adjusted to reflect the dynamic range (i.e., RS), latency, and jitter characteristics as were described in the group trends described in Section III. All the fibers' histograms were stored into a three-dimensional (fiber number x time bin x stimulus level bin) composite histogram. The contents of this array were then summed across the fibers to obtain the compound PST histogram. For each stimulus level, the compound PST histogram array was then convolved with a unit potential to produce the derived EAP. More details of these components are described below.

4.2.2 Single-fiber threshold histogram

An essential element of the model is the distribution of fiber thresholds across stimulus level. A challenge was to sample a sufficiently large number of fibers to achieve a reasonable estimate of this distribution. Small samples will tend to underestimate the range of single-fiber thresholds. This is seen in the three threshold histograms presented by van den Honert and Stypulkowski (1987, Fig. 4b) across which the threshold range increases with the number of fibers in each histogram. To maximize our sample, we combined single-fiber data of 230 fibers from 13 cats. The composite threshold histogram is shown in Fig. 6-A and was computed by using the normalized single-fiber thresholds as described above. The ratio of the highest and lowest fiber thresholds is about 15, or about 23.5 dB. Included in Fig. 6-A are two smooth fits to the data. The dotted line represents a "log-normal" (i.e., gaussian fit with a logarithmic transformation of the x-axis) least-squared-error fit. While this was a reasonable fit (r=0.98), it yielded positive residuals at both tails. This error was reduced by modifying the tails by fitting decaying exponentials to each tail region. This modified log-normal fit was used to provide interpolated values in our model simulations. We include for comparison (Fig. 6-B) the histogram obtained by van den Honert and Stypulkowski (1987) from their cat that yielded the largest number of fiber thresholds. Their function has the same overall shape a peaked and

skewed function with a high-level tail. The ratio of the highest and lowest threshold was reported as 9.9, or about 20 dB.

4.3 Modeling the post-stimulus-time histograms

In the simulations, PST histograms were modeled for each fiber at several stimulus levels covering the dynamic range of each fiber. This was done by creating a set of functions fit to a set of PST histograms of an archetypal fiber. The single fiber data chosen for these fits fulfilled two criteria. First, we required PST histograms obtained at several stimulus levels so as to represent a wide range of FE's. Second, the fiber's action potential waveforms had to suffer little contamination from electrical stimulus artifact or that from recorded EAP potentials. Contamination from either could skew estimates of latency and jitter. The chosen, archetypal fiber had negligable contaminants and yielded PST histograms covering FE's ranging from 22 to 100

Weibull functions (e.g., Hahn and Shapiro, 1967) were chosen as a convenient way to model the histograms, since their four parameters enabled us to independently control the amplitude, standard deviation (i.e., jitter), and time-axis offset (i.e., latency). Appropriate Weibull function parameters were determined empirically by using the Marquardt-Levenberg algorithm for a series of PST histograms obtained from the archetypal single fiber at several stimulus levels. These fits to the experimental data are shown by the solid lines of Fig. 7. The four Weibull parameters defining each fit were then plotted as functions of stimulus level. These scatter plots were, in turn, fit to smooth curves so that Weibull-fit histograms could then be computed for arbitrary stimulus levels.

4.4 Assigning mean latency, jitter, and relative spread characteristics to each modeled fiber

As described in Section III, the three single-fiber measures of mean latency, jitter, and relative spread were found to vary with fiber threshold across the fiber population. We therefore sought to model these level-dependent effects in the model. Second-order linear regression fits were used to estimate mean latency, jitter, and RS of each modeled fiber as a function of stimulus level. These values were then used to adjust the parameters of the Weibull functions used to model the PST histograms of each fiber.

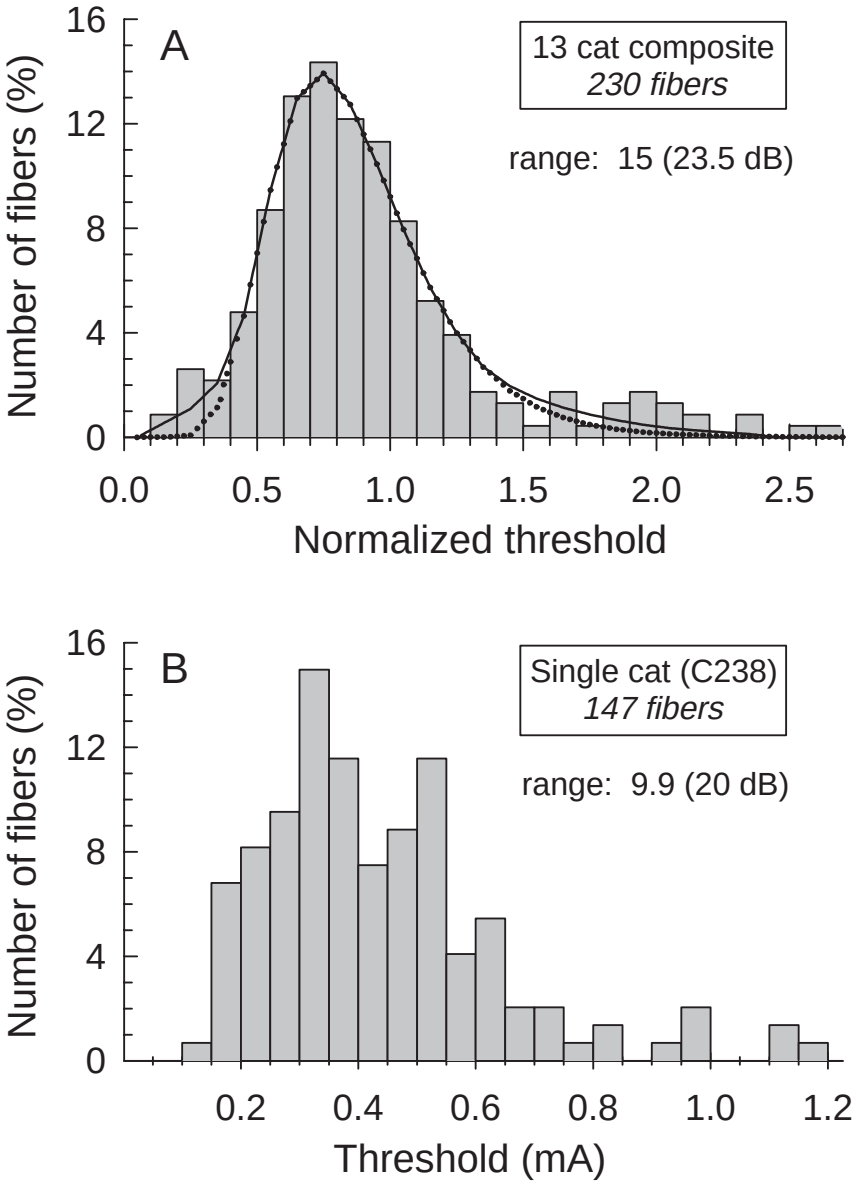

Figure 6: Single-fiber threshold distributions. The top distribution (A) was derived from the threshold data of the 13 cats of this study. In order to combine those data into a single histogram, thresholds (in linear current steps) were first normalized to the stimulus level yielding an EAP amplitude one-half that of the saturation value. The data are shown fit by a log-normal function (dotted line) and a modified form of the log-normal function (solid line), as discussed in the text. Linear (equal-width) threshold bins were used to construct our histogram. This facilitated comparison with data collected from a single cat by van den Honert and Stypulkowski (1987, Fig. 4-b), shown in panel B. The range indicated in each graph is the ratio of the maximum and minimum thresholds of each distribution.

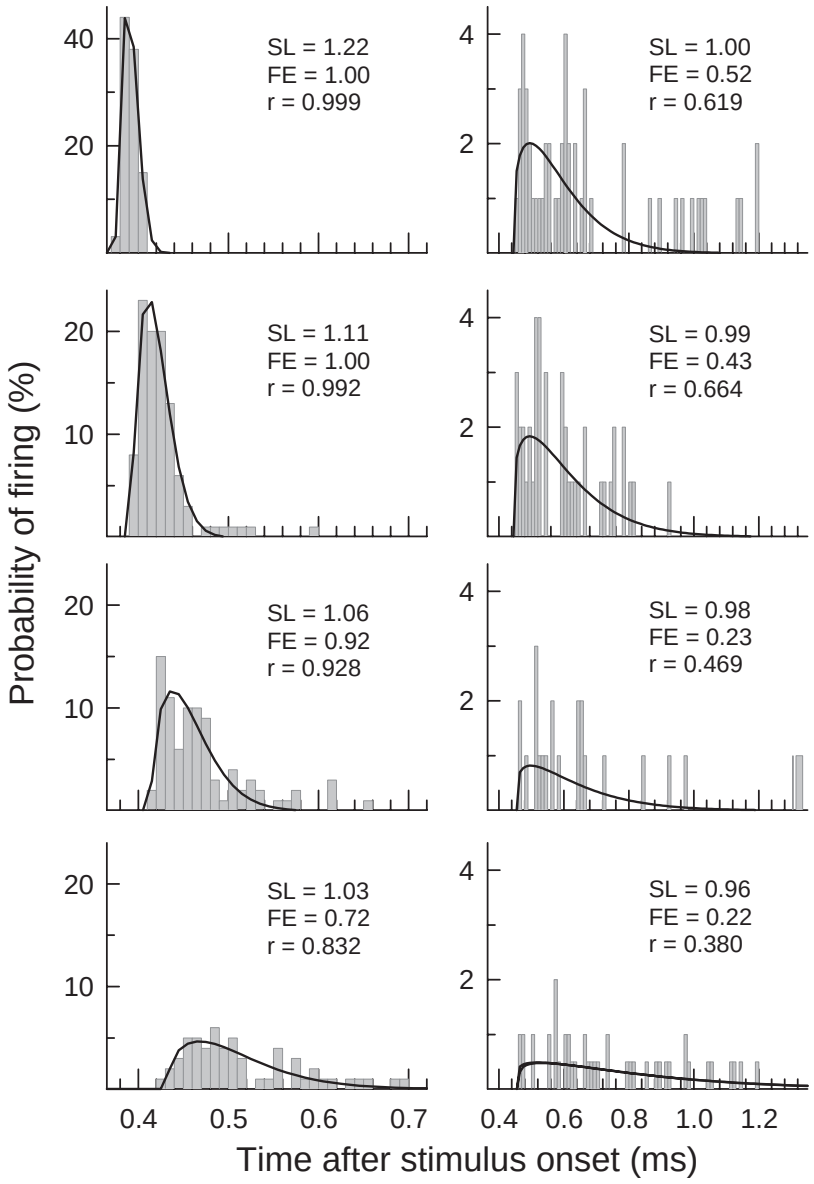

Figure 7: PST histograms from a selected "archetypal" fiber (bars) and corresponding Weibull function fits (solid lines) used in the model. The histograms (from fiber C39-01-03- 1) are arranged in two columns by stimulus level (SL), which was normalized to the level producing a firing efficiency (FE) of 50 %. Also shown in each graph is correlation coefficient (r) of each fit. Each Weibull function was defined by four parameters as described in Appendix A. These parameters were systematically varied as a function of stimulus level, enabling us to generate Weibull functions (i.e., modeled PST histograms) at arbitrary stimulus levels within the range covered by the experimental data. Note that different axes scales are used across the graphs.

4.5 Computation of the compound PST histogram

All computations were realized using Matlab (version 5.2) run on a Windows NT platform. The model was based upon simulating 1000 fibers. Post-stimulus-time histograms were realized in 5 ms time steps ranging from 0.35 to 2 ms. Stimulus levels ranged from 0.09 to 3.4 mA using a total of 97 increments. Across this stimulus range, the increment size was progressively widened (from 4 to 100 mA) to afford highest resolution at low stimulus levels. Thus, in computing the compound PST histogram, 97 histograms were computed for each fiber. At each stimulus level, the histograms of all 1000 fibers were summed to produce the compound PST histogram. Fig. 8-A shows a three-dimensional view of the compound PST histograms generated by the model. Histograms are plotted both as a function of post-stimulus time and stimulus level. In Fig. 8-B, specific compound histograms obtained at several different stimulus levels are shown to demonstrate greater temporal details.

4.6 The unit potential waveform

Following the method of Goldstein and Kiang (1958), the EAP at a given stimulus level was derived by convolving the compound PST histogram, obtained at that level with a "unit potential". That is,

$$A(t) = \int_{-\infty}^{t} P(\tau)U(t-\tau)d\tau \tag{1}$$

where A(t) is the gross potential (EAP), P(t) is the compound PST histogram, and U(t) is the unit potential. The unit potential is the voltage waveform, recorded by the EAP recording electrode, contributed by a single neuron. A key simplifying assumption made here is that all neurons of the nerve contribute equally; that is, U(t) is identical for all fibers. At least two across-fiber factors could contribute to unequal unit potentials: variations in fiber diameter and differences in fiber-to-electrode distance. However, diameters of afferent fibers in the cat have been shown to be distributed over a narrow range (Arnesen and Osen, 1978). Furthermore, axon diameter is not strongly correlated with characteristic frequency (Liberman and Oliver, 1984). These findings suggest that, along the baso-apical dimension of the cochlea, the fiber diameters of different regions of cochlear innervation would be comparable.

With an EAP recording electrode positioned directly on the nerve, we might suspect significant variation in fiber-electrode distance. Due to the

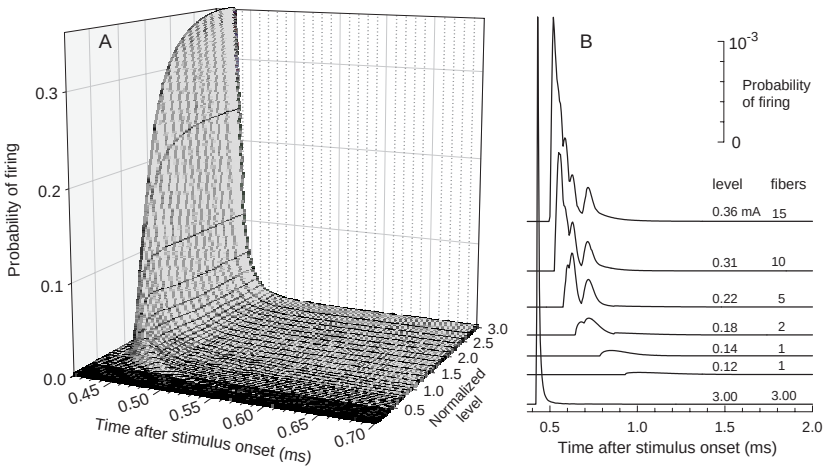

Figure 8: Compound post-stimulus-time histograms produced by the model, illustrating the summed, temporal firing pattern of all modeled fibers. Figure A illustrates 50 histograms selected over the dynamic range of all fibers. The stimulus level step size was varied across that range to show detail at low levels. Figure B illustrates several compound histograms computed for low stimulus levels. The six histograms representing levels from 0.12 to 0.36 mA are all plotted using the vertical scale indicated. Also shown (bottom trace) is the histogram created at 3.0 mA, a level at which all histograms reached their final (saturated) state. That trace is plotted on a vertical scale 1/150th of that of the others. The ripples appearing in some histograms are artifacts of the limited number of fibers in the model.

cochleotopic organization of auditory nerve fibers (Sando, 1965; Arnesen and Osen, 1978), we might hypothesize a relatively greater unit contribution from fibers innervating the basal turn of the cochlea. In that case, EAP measures obtained with such electrode placement would disproportionately represent basal fibers. We examined this issue in a cat preparation by recording an EAP amplitude-level function at three different recording sites, one directly on the surface of the nerve and two more distant (i.e., 2 and 4 mm) from the surface. Our conjecture was that if a fiber-electrode distance function existed, the shape of the amplitude-level functions from the three sites would vary. In that case, we would then assume that the electrode positioned directly on the nerve received different relative contributions from each fiber than did more distantly placed electrodes. The results from that experiment demonstrated growth functions from the three sites that were comparable, suggesting that the unit potentials contributed by different fibers within the nerve do not greatly differ under our experimental conditions. While the results of this preliminary study do not rigorously address all the issues involving the unit potential, they suggest that our assumption of a constant unit potential does not grossly distort the modeling results.

Our unit potential waveform was derived by solving Equation 1 for U(t). This was done first by Fourier transformation of Equation 1, solving for U(f), and then performing the inverse transform to obtain U(t). For this solution, A(t) was chosen as an EAP waveform obtained at a stimulus level near the saturation level of its amplitude- level function. Likewise, P(t) was chosen as a composite PST histogram obtained at the maximum modeled stimulus level. The archetypal EAP waveform was selected from among several cats yielding waveforms relatively free from stimulus artifacts. Among those waveforms, the EAP from subject C40 was chosen on the basis of its short interpeak (i.e., N1 to P2) latency. We considered short interpeak latency desirable, since it could reflect relatively little temporal dispersion of the waveform. The high-level PST histogram used in the solution for U(t) closely approximated an impulse function, as can be seen below in the high-level compound histogram of Fig. 8-B. Thus, the waveform of U(t) very closely resembles the high-level archetypal EAP waveform from cat C40.

4.7 Results

4.7.1 Compound histograms and derived EAP waveforms

As introduced above, Fig. 8 shows the compound PST histograms generated by the model. It is worth noting that, at low stimulus levels, the compound histograms demonstrate considerable dispersion and long latencies. Also, some exhibit a series of peaks or ripples in the downward slope of the histogram, as is readily seen in Fig. 8-B. These ripples are artifacts of the limited number of fibers in the model: they represent individual fibers whose histograms have approached their final and unique minimum values for latency and jitter.

Results of convolution of the compound PST histograms and the unit potential are shown in Fig. 9. The top panel (A) shows representative derived EAP waveforms and the lower panels (B) show latency-level and amplitude-level functions. Included in the plots are input-output functions obtained from 16 cats using monophasic cathodic stimuli presented to an intracochlear monopolar electrode. The experimental cat data have been normalized in two ways to facilitate comparisons across the cats, as well as with the model data: 1) amplitudes were normalized to the maximum (saturation) amplitude and 2) stimulus levels were normalized to the level at which amplitude reached 50However, there are some discrepancies in both the latency and amplitude functions. Compared to the mean experimental N1 latency-level data, the model curve is displaced upward to higher latencies. Also, the experimental latencies continue to decrease as saturation levels are reached, whereas the model curve reaches a horizontal asymptote. The modeled P2 latency function predicts the experimental EAP data reasonably well at high stimulus levels, but underestimates latency at low levels. Finally, the model amplitude-level curve overestimates amplitude over most of its dynamic range. At stimulus levels of about 1.25 and greater, the model underestimates the slope of the amplitude-level functions.

4.7.2 Comparisons with alternative models

This model provides the opportunity to compare its "full model" output (i.e., the amplitude-level function of the derived EAP waveforms) with simpler models based only on fiber thresholds and total spike count. This is a useful aspect of the model since it can help determine the aspects of the underlying neural responses that are most salient to the gross, EAP, potential. These simpler model outputs were generated as a result of computing the "full

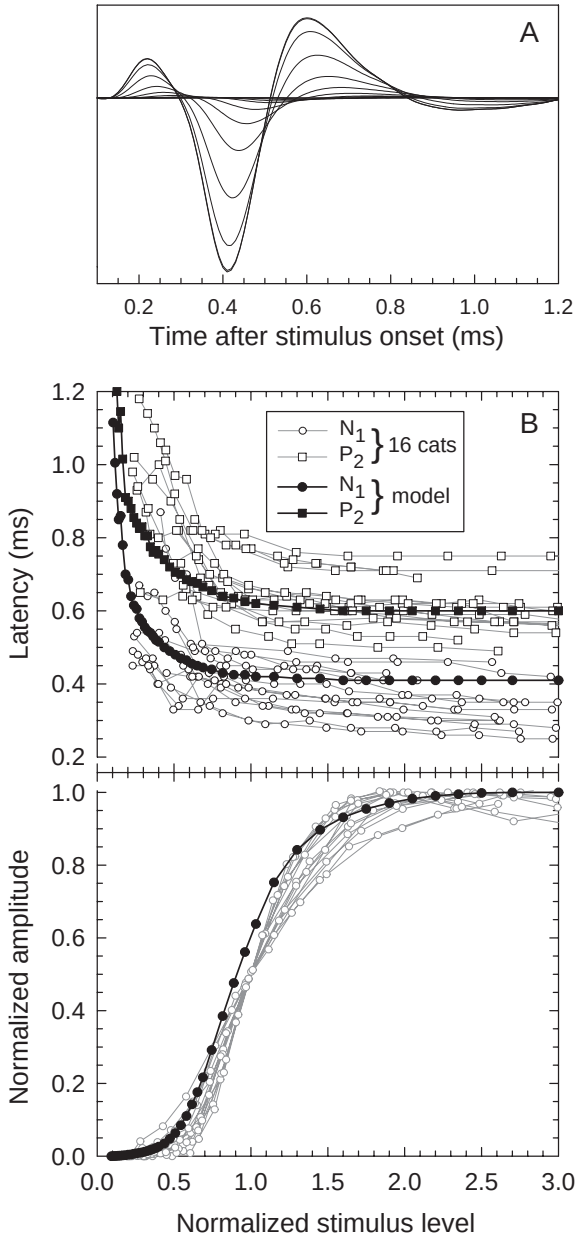

Figure 9: EAP waveforms (A) and input-output functions (B) produced by the model. Representative EAP waveforms obtained at several stimulus levels are shown in panel A. In panel B, modeled latency-level and amplitude-level functions are plotted with filled symbols, while experimental data from 16 cats are plotted with open symbols. The N1 peak is defined by the most negative point of the waveform and the P2 peak as the subsequent maximum. Stimulus level and amplitudes are normalized as described in the text.

model" output.

The *threshold* model is simply the integral of the fiber threshold distribution, equivalent to the cumulative threshold distributions shown by van den Honert and Stypulkowski (1987, Fig. 4-a). A *stochastic* model is based on the summation and integration of all fibers' PST histograms at each stimulus level. Thus, while it accounts for the stochastic nature of each fiber's input-output function, it ignores the temporal aspect that is included in the full model. In other words, the stochastic model assumes that all fibers respond with the same latency and with no jitter. Both of these simpler models were derived from intermediate outputs of the full model. Input-output functions produced by the "threshold", "stochastic", and "full" models are shown in the left column of Fig. 10. When plotted on linear axes (Fig. 10-B), the threshold and stochastic model outputs appear to be virtually identical, with the threshold model data superimposed over that of the stochastic model. The threshold and stochastic models overestimate both the full model and the actual EAP functions. The threshold and stochastic model output maintain their close correspondence at very low stimulus level, as evidenced by comparison of the data plotted on log-log axes (Fig. 10-C). The stair-step pattern in the threshold model data at low levels is due to the limited number of modeled fibers. At the lowest levels, there is relatively greater divergence between those two model outputs and that of the full model.

4.7.3 Effect of manipulating fiber threshold distribution

The close correspondence observed between the outputs of the threshold and stochastic models is dependent upon the slope of the threshold distribution function. A greater slope would presumably result in a greater deviation between the two model outputs. This was investigated by altering the threshold distribution of our model. The distribution was compressed by decreasing the scale of the threshold axis by 50% while maintaining the same value of the distribution's mode (Fig. 10-D). The results of this manipulation are shown in the plots of the right column of Fig. 10. All three model outputs now greatly overestimate the slope of the experimental EAP amplitude- level functions (Figs 10-E and 10-F). Note that, at the low stimulus levels (best observed in Fig. 10-F), the threshold model fails to account for the neural responses produced by the stochastic and full models. Using the levels producing the minimal responses (arrows in Fig. 10-F), the stochastic model produced a response at level 3.3 dB lower than did the threshold model. Thus, under the condition of a compressed threshold dis-

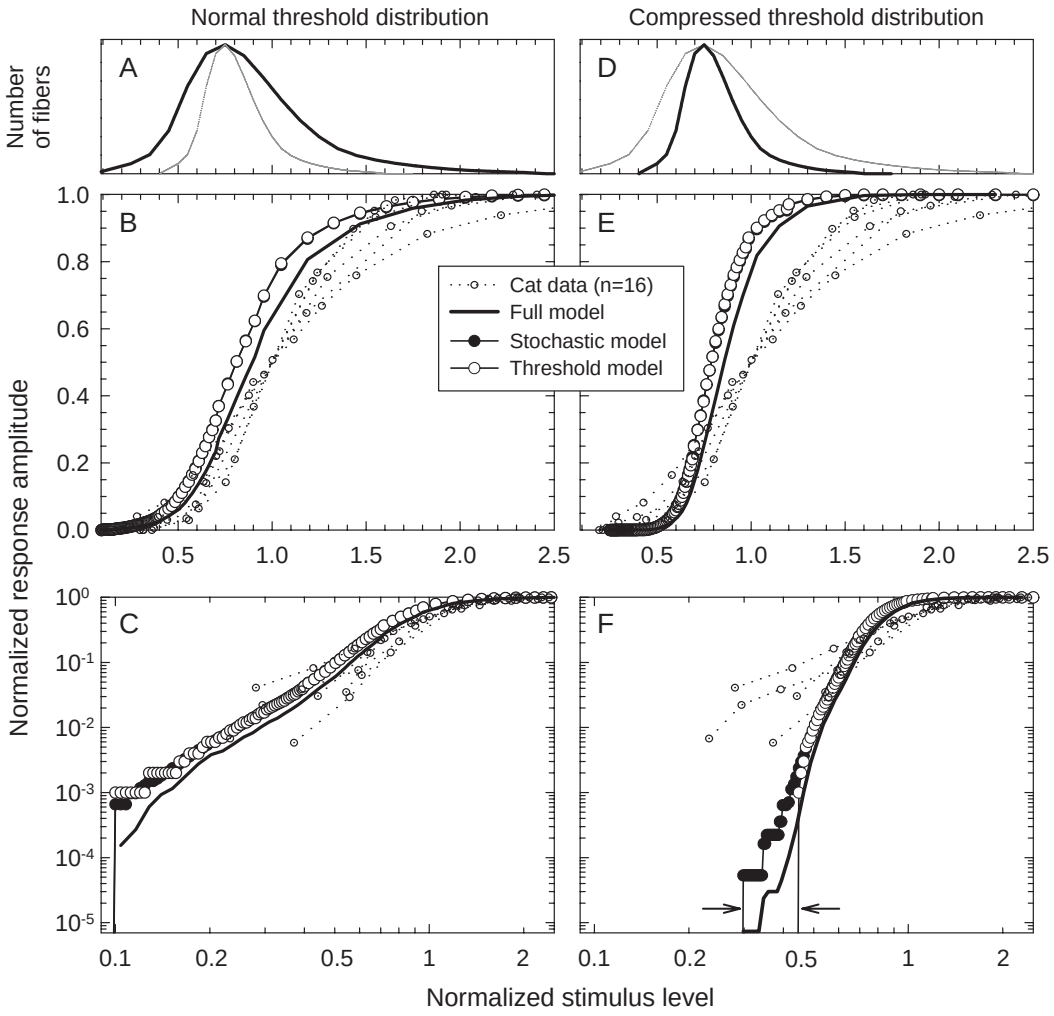

Figure 10: Comparison of model results using two different fiber threshold distributions. The input-output functions in left column (B and C) were computed using the same threshold distribution (A) as was used in deriving the data of Fig. 9. The data shown in the right column (E and F) were obtained from a narrower threshold distribution (D) by compressing the distribution of panel A by 50%. Various model outputs are plotted on linear axes in panels B and E for the normal and compressed threshold distributions, respectively. For greater clarity at low levels, the same data are plotted on logarithmic axes in panels C and F. Also shown in these plots are the experimental data obtained from 16 cats. In addition to the data from the full model, input-output functions from simpler models ("Stochastic" and "Threshold") are plotted for comparison. The arrows in panel F denote the minimum stimulus levels for which a non-zero response was output by the stochastic and threshold models.

tribution, the addition of the stochastic fiber property of relative spread enhances the dynamic range of the EAP amplitude-level function. Note, however, that, with the compressed threshold distribution, all three models deviated significantly from the results obtained from the experimental data, as can be seen in Fig. 10-E and 10-F.

4.8 Concluding remarks

We have presented a computational model that provides a phenomenological description of how the population of single-fiber responses integrate to produce the whole nerve response. When compared directly with EAP input-output functions obtained from experimental preparations, the model does so with reasonable accuracy. The model presented here demonstrates that the underlying distribution of single-fiber thresholds plays a fundamental role in determining the shape of the EAP amplitude-level function. As demonstrated in Fig. 10, other single-fiber parameters such as jitter and RS have relatively little impact on this function. This underscores the importance of accurate threshold distributions in such modeling efforts.

We have also illustrated how model parameters can be manipulated to investigate the effects of various parameters, such as the width of the threshold distribution. As was shown in Fig. 10, other fiber parameters (such as RS) can have significant effects on the growth of the EAP under conditions where the fiber threshold distribution is compressed. Such compression may indeed occur in pathological ears and therefore underscore the importance of considering multiple single-fiber attributes (i.e., threshold, RS, and temporal properties) when modeling responses from pathological ears.

5 Plans for next quarter

Plans for the tenth quarter include the following:

- Process histology and analysis on chronically deafened cat and guinea pig experimental subjects recently completed.
- Perform additional acute physiological (EAP) measures and histological analyses on chronically deafened guinea pigs.
- Make three podium presentations on material directly related to our contract at the Midwinter Meeting of the Association of Research in Otolaryngology, St. Petersburg Beach, Florida.

- Revise and submit a manuscript on basic single-fiber response properties for publication.
- Prepare an invited book chapter "How do cochlear prostheses work" for **Current Opinion in Neurobiology Vol 9/4**.

6 References

Goldstein, M.H. and Kiang, N.Y-S (1958) Synchrony of neural activity in electric responses evoked by transient acoustic stimuli. J. Acoust. Soc. Am. 30, 107-114.

Hahn, G.J. and Shapiro, S.S. (1967) Statistical models in engineering New York, John Wiley & Sons.

Kiang, N. Y-S, Moxon, E.C., and Levine, R.A. (1970). Auditory nerve activity in cats with normal and abnormal cochleas. In Sensorineural Hearing Loss, Ciba Symposium, G.E.W. Wolstenholme and J. Knight eds, (J. and A. Churchill, London), pp 241-273.

Kiang, N. Y-S, Moxon, E.C., and Kahn, A.R. (1976) The relationship of gross potentials recorded from the cochlea to single unit activity in the auditory nerve. In R.J. Rubin, C. Elberling, and G. Salomon (eds.) Electrocochleography. Baltimore, University Park.

Liberman, M.C. and Oliver, M.E. (1984) Morphometry of intracellularly labeled neurons of the auditory nerve: correlations with functional properties. J. Comp. Neurol. 223, 163-176.

Rattay, F. (1986) Analysis of models for external stimulation of axons. IEEE Trans. Biomed. Eng. 33, 974-977.

Rubinstein, J.T., Wilson, B.S., Finley, C.C., an d Abbas, P.J. (1999) Pseudospontaneous activity: Stochastic independence of auditory nerve fibers with electrical stimulations. Hear. Res. 127, 108-118, 1999.

Shepherd, R.K., Hatsushika, S., and Clark, G.M. (1993) Electrical stimulation of the auditory nerve: The effect of electrode position on neural excitation. Hear. Res. 66, 108-120.

Spoendlin, H. and Schrott, A. (1989) Analysis of the human auditory nerve. Hear. Res. 43, 25-38.

van den Honert, C. and Stypulkowski, P.H. (1987) Single fiber mapping of spatial excitation patterns in the electrically stimulated auditory nerve. Hear. Res. 29, 195-206.

Verveen, A.A. (1961). Fluctuation in Excitability, Drukkerij, Holland N.V., Amsterdam.

Wang, B. (1979) The relation between the compound action potential and unit discharges of the auditory nerve. Ph.D. thesis, Massachusetts Institute of Technology, Cambridge, Massachusetts.

Wang, B. and Kiang, N.Y.S. (1978) Synthesized compound action potentials (CAPs) of the auditory nerve. J. Acoust. Soc. Am. 63 (Suppl.), S77.